




**Please cite the Published Version**

Gomis-Berenguer, Alicia , Casanova, Ana , Banks, Craig E  and Iniesta, Jesús (2024) All-in-one continuous electrochemical monitoring of 2-phenylphenol removal from water by electro-Fenton treatment. *Talanta*, 272. 125761 ISSN 0039-9140

**DOI:** <https://doi.org/10.1016/j.talanta.2024.125761>

**Publisher:** Elsevier BV

**Version:** Published Version

**Downloaded from:** <https://e-space.mmu.ac.uk/634560/>

**Usage rights:**  [Creative Commons: Attribution 4.0](https://creativecommons.org/licenses/by/4.0/)

**Additional Information:** This is an open access article which originally appeared in *Talanta*

**Data Access Statement:** Data will be made available on request.

**Enquiries:**

If you have questions about this document, contact [openresearch@mmu.ac.uk](mailto:openresearch@mmu.ac.uk). Please include the URL of the record in e-space. If you believe that your, or a third party's rights have been compromised through this document please see our Take Down policy (available from <https://www.mmu.ac.uk/library/using-the-library/policies-and-guidelines>)



# All-in-one continuous electrochemical monitoring of 2-phenylphenol removal from water by electro-Fenton treatment

Alicia Gomis-Berenguer<sup>a,\*</sup>, Ana Casanova<sup>b,\*\*</sup>, Craig E. Banks<sup>c</sup>, Jesús Iniesta<sup>a,d</sup>

<sup>a</sup> Institute of Electrochemistry, University of Alicante, 03080, Alicante, Spain

<sup>b</sup> Interfaces, Confinement, Matériaux et Nanostructures, ICMN-CNRS (UMR 7374) - Université d'Orléans, 1b rue de la Férollerie, 45071, Orléans, Cedex 2, France

<sup>c</sup> Faculty of Science and Engineering, Manchester Metropolitan University, Chester Street, Manchester, M1 5GD, UK

<sup>d</sup> Department of Physical Chemistry, University of Alicante, 03080, Alicante, Spain

## ARTICLE INFO

### Keywords:

2-Phenylphenol  
Carbon black  
Oxidised carbon black  
Electro-fenton  
Screen-printed carbon electrodes  
Electrochemical sensor

## ABSTRACT

The biggest allure of heterogeneous electro-Fenton (HEF) processes largely fails on its high efficiency for the degradation of a plethora of hazardous compounds present in water, but still challenging to search for good and cost-effective electrocatalyst. In this work, carbon black (CB) and oxidised carbon black (CBox) materials were investigated as cathodes in the electrochemical production of hydrogen peroxide involved in HEF reaction for the degradation of 2-phenylphenol (2PP) as a target pollutant. The electrodes were fabricated by employing carbon cloth as support, and the highest H<sub>2</sub>O<sub>2</sub> production yields were obtained for the CBox, pointing out the beneficial effect of the hydrophilic character of the electrode and oxygen-type functionalization of the carbonaceous surface. HEF degradation of 2PP was explored at  $-0.7$  V vs. Ag/AgCl exhibiting the best conversion rates and degradation grade (total organic carbon) for the CBox-based cathode. In addition, the incorporation of an electrochemical sensor of 2PP in line with the HEF reactor was accomplished by the use of screen-printed electrodes (SPE) in order to monitor the pollutant degradation. The electrochemical sensor performance was evaluated from the oxidation of 2PP in the presence of Fe<sup>2+</sup> ions by using square wave voltammetry (SWV) technique. The best electrochemical sensor performance was based on SPE modified with Meldola Blue showing a high sensitivity, low detection limit (0.12 ppm) and wide linear range (0.5–21 ppm) with good reproducibility (RSD 2.3 %). The all-in-one electrochemical station has been successfully tested for the degradation and quantification of 2PP, obtaining good recoveries analysing spiked waters from different water matrices origins.

## 1. Introduction

During the last decades, anthropogenic activities are becoming a significant threat to the global environment, and consequently, the continuous release of different types of pollutants into the aquatic media is leading to the dramatic deterioration of the surface water resource quality. These hazardous pollutants are, in general, persistent species that accumulate in the aquatic medium, provoking a high toxicological impact on the environment, and consequently, affecting the human health and the subsistence of living beings. The most common pollutants come from the industry activity and include, among others, dyes, heavy metals, pesticides, pharmaceuticals, personal care products, industrial additives, and agrochemicals [1,2].

2-phenylphenol (also named *ortho*-phenylphenol), 2PP, is a broad-

spectrum microbiocide, which belongs to the hydroxybiphenyl chemical family [3]. It is extensively employed as surface disinfectant in hospitals, houses, and laundries, as well as preservative (with E number E231) in wood and treatments of cosmetics, citrus fruit storage, and canned drinks [4,5]. Due to the wide use of this biocide, its detection has been reported in sediments, natural water [6,7], and even in prepared food (i.e., washed, peeled, cooked, etc.) [8]. Regarding 2PP toxicity, several studies have been revealing that could cause chronic toxicity to organisms by bioaccumulation. It can disrupt the endocrine system of both male and female organisms and possess carcinogenic and cytotoxic properties [9–11]. Accordingly, World Health Organization (WHO) established 0.4 mg/kg of body weight as an acceptable daily intake (ADI) for humans.

According to all the above, during the last decade different

\* Corresponding author.

\*\* Corresponding author.

E-mail addresses: [alicia.gomis@ua.es](mailto:alicia.gomis@ua.es) (A. Gomis-Berenguer), [ana.casanova-martinez@cnrs-orleans.fr](mailto:ana.casanova-martinez@cnrs-orleans.fr) (A. Casanova).

<https://doi.org/10.1016/j.talanta.2024.125761>

Received 17 October 2023; Received in revised form 29 January 2024; Accepted 6 February 2024

Available online 15 February 2024

0039-9140/© 2024 The Authors. Published by Elsevier B.V. This is an open access article under the CC BY license (<http://creativecommons.org/licenses/by/4.0/>).

remediation strategies are emerging, some of them consolidated, to reduce this compound concentration from aqueous media, through biodegradation [12], adsorption in porous materials [13,14] or chemical degradation [15,16]. In this regard, Hou et al. reported the adsorption mechanism of 2PP on various zeolites obtaining an adsorption capacity of 299.4 mg/g in a microporous zeolite [17]. Olak-Kucharczyk and co-workers reported the use of H<sub>2</sub>O<sub>2</sub>/UVC process consisting of the *in-situ* generated hydroxyl radicals, through H<sub>2</sub>O<sub>2</sub> photolysis, as main oxidants; the authors achieved 89 % of total organic carbon reduction after 2 h of reaction [18].

Among the chemical degradation methods of pollutants, heterogeneous electro-Fenton (HEF) processes emerged as an attractive electrochemical mechanism based on the *in-situ* electrogeneration of H<sub>2</sub>O<sub>2</sub> through a cathodic reduction of O<sub>2</sub> in acidic medium (equation (1)) and the subsequent generation of hydroxyl radicals by the Fenton reaction between the Fe<sup>2+</sup> species (present in solution) and H<sub>2</sub>O<sub>2</sub>, thus generating Fe<sup>3+</sup> (equation (2)) which is further reduced on the cathode maintaining the catalytic cycle (equation (3)) [19,20]. Finally, the hydroxyl radicals generated react with the organic pollutant (equation (4)).



As far as the electrochemical reaction (1), different electrodes have been investigated to promote the two-electron oxygen reduction reaction (ORR), being carbonaceous materials a good alternative for noble metal-based electrodes (e.g., Au- and Pt-based electrodes), due to their low cost, chemical stability, and environmental compatibility [21]. Nonetheless, carbon felt [22,23], reticulated vitreous carbon [24,25], carbon sponge [26], graphite [27] and even those carbon materials doped with heteroatoms (e.g., N-, O-, B-) [21,28–30] are some examples of the carbon materials employed as good electrocatalysts. Particularly, carbon blacks, formed through incomplete combustion of either gaseous or liquid hydrocarbons, are widely used as support or additive for electrodes in electrochemical applications (e.g., supercapacitors, batteries, polymer electrolyte membrane fuel cells, PEMFC) due to their high electrical conductivity, low cost, and reasonably high chemical stability [31,32]. More recently, its electrocatalytic performance towards two-electron ORR was reported to show interesting results [33–35].

Apart from the adequateness of cathode material and optimal HEF conditions to reach the pollutant degradation, exhaustive monitoring of the molecule and produced intermediates, in terms of cost-effectivity and real-time monitoring, is required to study the efficiency of the electrochemical process. In this sense, the most analytical tools employed for HEF reaction monitoring include external or *ex-situ* analytical procedures such as high-performance liquid chromatography (HPLC) either coupled with UV-Vis or mass spectrometry. However, these analytical techniques are highly solvent-dependent, sample destruction and time-consuming, as well as mostly expensive; additionally, in most cases, a sample pre-treatment is required (filtration and/or pH adjustment). Alternatively, electroanalysis is presented as a rapid (few minutes), sensitive, and majorly non-sample treatment method to follow a HEF reaction [36,37].

Despite the plethora of studies based on electro-Fenton (EF) process for the degradation of pollutants, scarce literature is found on its application for the degradation of 2PP. Currently, only Sanromán and collaborators reported an EF-like process in which they employed a transition metal as catalyst (Ni and Zn), showing a removal percentage of 80% before 1 h with optimal experimental conditions [38].

In this work, we first explore the conversion of the fungicide 2PP via EF reaction in an undivided electrochemical cell by comparing both a

commercial carbon black and the modified one by introducing oxygen-containing functional groups. The electrocatalytic activity of both carbon black based cathodes is examined toward the direct increase in the production rate of hydrogen peroxide and, therefore, indirectly degradation efficiency of 2PP and total organic carbon reduction in aqueous solutions under controlled potentials. Secondly, the all-in-one electrochemical device, including HEF station and electroanalysis one is developed. The aim is to couple the electrochemical cell to an electrochemical sensor based on screen printed electrode (SPE), which allows a fast and accurate evaluation of the grade of 2PP degradation under real-time conditions during HEF electrolysis. On this matter, the electrochemical sensor for the monitoring of 2PP solutions in the presence of iron (II) ions has been partially validated in terms of sensitivity, LoD, LoQ, repeatability and reproducibility, and the performance of the electrochemical sensor is compared to conventional chromatographic method. Finally, the all-in-one system has been tested for pollutant degradation in three spiked real waters.

## 2. Materials and methods

### 2.1. Materials and reagents

All chemicals commercially available were used without further purification. Analytical grade polytetrafluoroethylene (PTFE, 60 wt. % dispersion in H<sub>2</sub>O), potassium titanium oxide oxalate dihydrate (K<sub>2</sub>C<sub>4</sub>O<sub>9</sub>Ti·2H<sub>2</sub>O, ≥90 %), sodium sulfate (Na<sub>2</sub>SO<sub>4</sub>, 98 %), and iron (II) sulfate heptahydrate (FeSO<sub>4</sub>·7H<sub>2</sub>O, puriss p.a.), Nafion (5 % in water) were purchased from Sigma Aldrich. Acetone (≥99 %), ethanol absolute (96 % v/v), acetonitrile (≥99.9 %), and sulfuric acid (H<sub>2</sub>SO<sub>4</sub>, 98 %) were purchased from VWR. 2-phenylphenol (99 %) was supplied by Thermoscientific. All aqueous solutions were prepared using doubly deionized water (DIW), not less than 18.2 MΩ cm, purified by Milli-Q water system.

The carbon cloth was purchased from E-TEK with a thickness of 0.40 mm and no wet proofing. Before use, carbon cloth was cleaned by mechanical sonication in acetone using an ultrasound bath for 30 min, and then the same procedure was followed in water, and finally dried at 80 °C for 12 h. A piece of carbon cloth with 5.5 × 4.5 cm dimensions was used as a substrate for the carbonaceous electrode preparation which involved the dip coating into carbon black materials dispersion.

Carbon black (Vulcan XC72R) was supplied by Cabot and named as CB. For the mild oxidation of CB, 2.0 g was placed on 200 mL of concentrated HNO<sub>3</sub> (≥65 %), and heated under reflux at 120 °C under vigorous stirring for 90 min. After the oxidation treatment, the obtained material was filtered, then thoroughly washed with DIW, and dried at 60 °C for 12 h; the sample was named CBox.

### 2.2. Cathodes preparation

The ink for the fabrication of cathodes used in the HEF process consisted of mixing the carbonaceous material (CB or CBox) in a concentration of 2 mg/mL and PTFE as binder in a concentration of 5 mg/mL in a 1 to 2.5 ratio v/v of EtOH:H<sub>2</sub>O. Successively, the carbon cloth pieces were submerged in the ink solution and sonicated in an ultrasound bath for 30 min in order to get a homogeneous impregnation. Then, the impregnated carbon cloths were dried at 80 °C for 12 h and annealed at 350 °C in a muffle for 30 min. For comparative purposes, a carbon cloth was impregnated with PTFE (in the absence of carbonaceous material). The resulting modified carbon cloths account for CC-PTFE, CC-CB, and CC-CBox. With regards to the HEF, the modified carbon cloth electrodes were held up in a homemade electrode holder and a titanium wire was employed to make the electrical connection.

### 2.3. Characterization techniques of materials

Since the thermal treatment applied for the cathode's preparation

(see section 2.2) is expected to modify the surface chemistry of the material (Fig. S1), prior to material characterization, a thermal pretreatment (350 °C for 30 min) was carried out to CBox to mimic the final material present on the cathodes.

The surface pH was determined by measuring the pH of equilibrated aqueous suspensions (ca. 1.0 g/L stirring for 72 h) of each material. Thermogravimetric analysis (TG) was carried out using a thermogravimetric analyser from Netzsch. Experiments were carried out under an argon flow rate of 50 mL/min at a heating rate of 10 °C/min, up to a final temperature of 900 °C. For each experiment, about 20 mg of sample was used. As far as temperature-programmed desorption coupled with mass spectrometry (TPD-MS) experiments, the gas phase (CO and CO<sub>2</sub>) was continuously monitored by MS.

X-ray photoelectron spectroscopy (XPS) was performed with a K-ALPHA spectrometer (Thermo Scientific, Waltham, MA, USA). Each spectrum was recorded using Al-K $\alpha$  radiation (1486.6 eV), monochromatized by a twin crystal monochromator, generating a focused X-ray spot with a diameter of 400 nm, at 3 mA  $\times$  12 kV. The alpha hemispherical analyzer was set to the constant energy mode with survey scan pass energies of 200 eV to access the whole energy band and 50 eV in a narrow scan.

The electrochemical characterization of the CB and CBox supported on glassy carbon electrode (GCE, 3.0 mm diameter) and glassy carbon rotating disk electrode (RDE, 3.0 mm diameter) was carried by cyclic voltammetry (CV) and linear sweep voltammetry (LSV), respectively. An ink consisting of a suspension of 5 mg/mL of each carbon black (CB and CBox) in ethanol in the presence of 1.5 % of Nafion (total loading of ca. 0.7 mg/cm<sup>2</sup>) was drop-casted layer by layer on top of the GCE and let dry overnight in air. The electrodes were labelled as GCE-CB and GCE-CBox, and RDE-CB and RDE-CBox for GCE and RDE, respectively.

The CV and LSV responses were recorded by using a VMP-3e multichannel potentiostat/galvanostat (Biologic-EC-Lab) in a 3-electrode cell configuration using GCE-CB or GCE-CBox as working electrode, a graphite rod, and Ag/AgCl (3 M KCl) via luggin as counter and reference electrodes, respectively. Electrochemical experiments were performed at room temperature and in triplicate.

#### 2.4. Electrochemical assays

HEF assays were carried out at controlled potential (−0.7 V vs. Ag/AgCl) in an undivided electrochemical cell containing 200 mL solution with 20 ppm 2-phenylphenol and 0.2 mM of FeSO<sub>4</sub> in 50 mM Na<sub>2</sub>SO<sub>4</sub> as a supporting electrolyte. The pH was previously adjusted to 3.0 by adding a few drops of 1 M H<sub>2</sub>SO<sub>4</sub> (the resulting solution displays an ionic conductivity of 850.0  $\mu$ S/cm). The CB- and CBox-based electrodes were used as working electrode (cathode), while a single junction Ag/AgCl (3.0 M KCl) via luggin and a boron-doped diamond (BDD) sheet (3.5  $\times$  2.5 cm) were employed as reference and counter (anode) electrodes, respectively. The cathode and anode were arranged in parallel with an interelectrode gap of 6.0 cm. Prior to HEF measurements, the electrochemical cell was O<sub>2</sub>-saturated by bubbling the aqueous solution with a flux of oxygen (99.7 %) for 30 min; thereafter, a continuous O<sub>2</sub> bubbling in the vicinity of the cathode was maintained together with stirring by using a magnetic bar in order to promote the mass transfer of dissolved O<sub>2</sub> from the bulk to the interface electrode/electrolyte. Likewise, a similar electrochemical setup is followed for the H<sub>2</sub>O<sub>2</sub> electro-generation by

using 50 mM Na<sub>2</sub>SO<sub>4</sub> as a supporting electrolyte at pH 3.0 at different selected potentials (−0.5 to −1.0 V vs. Ag/AgCl). As far as the cathode stability test, six consecutive HEF reactions were carried out under the same experimental conditions.

For the electrochemical experiments with real water, three matrices from different sources (tap, spring, and irrigation water) were spiked with 20 ppm of 2PP. The ionic conductivity and solution pH were adjusted if necessary (with Na<sub>2</sub>SO<sub>4</sub> and H<sub>2</sub>SO<sub>4</sub>) to mimic the experimental conditions described above. The main parameters of as-received real waters are collected in Table 1.

Before all H<sub>2</sub>O<sub>2</sub> electro-generation and HEF experiments, electrodes were soaked in 50 mM Na<sub>2</sub>SO<sub>4</sub> for 24 h to ensure the diffusion of the electrolyte into the carbon-based electrode network.

#### 2.5. Analytical methods

The electrocatalytic generation of H<sub>2</sub>O<sub>2</sub> was followed through the titanium oxalate complexation method [39]. Briefly, aliquots of 1.5 mL were taken from the electrochemical cell at specific intervals time until 2 h; all aliquots were subsequently mixed with 0.65 mL of H<sub>2</sub>SO<sub>4</sub> (385 g/L) and 0.35 mL of potassium titanium oxalate dihydrate solution (50 g/L). Once the reaction was completed (ca. 1 min), the solution turned yellow colour as a result of the formation of the Ti(IV)–H<sub>2</sub>O<sub>2</sub> complex. The complex concentration was recorded by UV–Vis spectrophotometry at 400 nm (maximum absorbance) using a Shimadzu spectrophotometer (UV–2401PC). Reading absorbance values were transformed into concentration according to the previous calibration curve made using known H<sub>2</sub>O<sub>2</sub> concentration solutions.

The HEF performance was assessed by both chromatographic and electroanalytical methods by following the 2PP concentration. As far as chromatography analysis, aliquots of 2 mL sample were taken from the electrochemical cell (the total solution volume was corrected for concentration calculations after aliquot withdrawal), and then filtered through a PTFE syringe filter (0.22  $\mu$ m). Samples were analysed by HPLC (Agilent) equipped with a diode array detector (DAD) using a reverse-phase column (Poroshell 120, EC-C18, 3.0  $\times$  100 mm, particle size of 2.7  $\mu$ m), with a mobile phase water (0.1 % formic acid): acetonitrile (40:60 v/v) and a flow rate of 0.4 mL/min. The column was thermostated at 30 °C and the injection volume was 20  $\mu$ L. 2PP peak was recorded at a wavelength of 245 nm exhibiting a retention time of 2.7 min. Simultaneously, total organic carbon (TOC) measurements were recorded on the solutions in a TOC-CV Shimadzu analyser.

Alternatively, the electroanalytical measurements of 2PP concentration were carried out in two types of homemade screen-printed carbon electrodes [40] with a three-electrode configuration system using silver/silver chloride (Ag/AgCl, C61003P7 Sun Chemical, South Normanton, UK) and carbon graphite (C2000802P2, Sun Chemical, South Normanton, UK) for the reference and counter electrodes, respectively. In the case of the working electrodes, two different carbon-based inks were employed: graphene (SPE-G, from JE Solutions Consultancy Ltd) or Meldola Blue (SPE-MB, C2030519P5 Sun Chemical, South Normanton, UK). CV and square wave voltammetry (SWV) techniques were used to explore the electrochemical response of 2PP at both SPEs. The electroanalytical detection of 2PP was followed by SWV from −0.3 to +0.8 V vs. Ag/AgCl. Optimal SWV parameters were the following: modulation amplitude, 100 mV; frequency, 8 Hz; modulation step, 2 mV.

**Table 1**  
Origin and main parameters of the different water samples employed in this work.

Water sample	Origin	Conductivity ( $\mu$ S/cm)	pH	Chloride (ppm)	NO <sub>2</sub> <sup>-</sup> /NO <sub>3</sub> <sup>-</sup> (ppm)	TOC (ppm)
DI water (DIW)	Milli-Q water system	1.2	6.0	n.d.	n.d./n.d.	n.d.
Tap water (TW)	Alicante, Spain (38.3808°N, −0.5239°W); May 2023	847.0	8.1	356	n.d./7.11	n.d.
Irrigation water (IW)	Murcia, Spain (38.0373°N, −1.0727°W); March 2023	2640.0	8.3	817	n.d./58.00	2.00
Spring water (SW)	Huesca, Spain (42.6630°N, 0.3212°W); June 2023	183.7	7.8	n.d.	n.d./0.59	n.d.

n.d.: Non detected.

The concentration of nitrate, nitrite, and chloride ions present in real water samples was analysed by ion chromatography (Metrohm) using an anion exchange column (MetroSep A Supp 4, Metrohm) of  $250 \times 4.0$  mm and a particle size of  $9 \mu\text{m}$ . The eluent was made of  $\text{Na}_2\text{CO}_3$  (1.8 mM)/ $\text{NaHCO}_3$  (1.7 mM) pumped at 1 mL/min. Detection of ions was performed by monitoring ionic conductivity with chemical suppression.

### 2.6 Experimental all-in-one set-up.

The all-in-one electrochemical station consisted of two main units, the HEF reactor coupled with an in-line cell for the 2PP degradation monitoring (Scheme 1, Fig. S2). The cell was designed with Solidworks software and fabricated using Clear resin (supplier reference: FLGPCL04) -stable under acidic media- in a Formlabs Form 3D printer. The screen-printed electrode was inserted into the internal reservoir (ca. 10 mL) of the cell through an upper slot and was employed for the 2PP concentration monitoring. To do so, the reservoir was continuously fed with the treated solution, containing  $2\text{PP-FeSO}_4\text{-Na}_2\text{SO}_4$ , from the HEF cell using a peristaltic pump. At certain times of reaction, the flow was stopped, and the electroanalytical measurement based on SWV was taken by using the SPE into solution. Prior to SPE integration into the cell, the 2PP calibration curve of each electrode was made.

## 3. Results and discussion

The first section of this manuscript deals with the characterization of the carbonaceous materials employed for the formulation of the inks and further the HEF cathodes preparation for the generation of  $\text{H}_2\text{O}_2$ . The identification of experimental conditions towards high current efficiency and production of  $\text{H}_2\text{O}_2$  is crucial for an HEF process, so the second part of the manuscript is devoted to the 2PP degradation, as a model hazardous fungicide, aiming to explore the feasibility of modified-carbon cloths. In this regard, the effect of the CB surface chemistry on the  $\text{H}_2\text{O}_2$  electrogeneration and, therefore, on the final 2PP degradation efficiency was explored. The development of an electrochemical sensor to detect 2PP is not an easy task and therefore requires a more exhaustive study in terms of choice of appropriate materials and electrochemical devices. To do so, the electrochemical sensing of 2PP is addressed based on electrochemical characterization of two different SPEs towards 2PP detection in the presence of iron (II) ions in solution which are involved in EF reaction. Under the best electroanalytical outcomes, the electrochemical sensor of 2PP is partially validated regarding sensitivity, linear range concentration, LoD, LoQ, repeatability, reproducibility, and its performance in real waters. Finally, the

all-in-one electrochemical station is proven for continuous monitoring of the pollutant degradation by applying a HEF process.

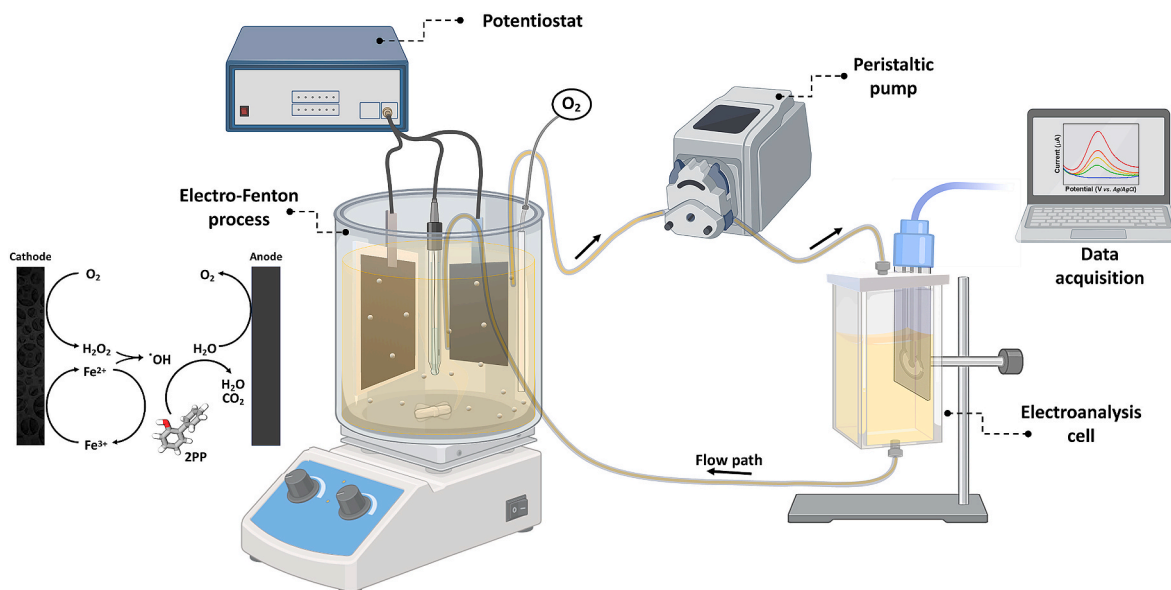
### 3.1. Characterization of carbonaceous-based materials and cathodes

XPS analysis was performed to assess the nature of the chemical modification of CB as a result of the oxidation treatment (Fig. S3). As far as both pristine CB and CBox, Fig. S3 reveals that the low binding energy component of the C 1s core level spectra, located at 284.6 eV is related to the graphitic carbon and the peak centered at 285.5–285.6 eV is associated with the aliphatic hydrocarbons. Additionally, the peaks located at 286.3–286.6 eV and 287.0–288.6 eV are assigned to  $-\text{C}-\text{O}$  and  $-\text{C}=\text{O}$  species, respectively. The O 1s core level spectrum of CB was composed of three main peaks in the range of 531.4–531.7, 532.9–533.4, 534.1–535.1 eV associated with  $-\text{C}=\text{O}$ ,  $-\text{C}-\text{O}$  and  $-\text{O}-/\text{O}-\text{C}=\text{O}$ , respectively [44]. Table 2 compiles the atomic percentage of C and O of pristine CB and CBox extracted from C 1s and O 1s core levels, those results reveal a low oxidised degree of CB that was remarkably increased after the acidic treatment rising from 1.7 to 8.5 at. % of O. It is worthy of note that N-containing groups were not incorporated into the material surface during nitric acid treatment. This fact is also important to discard the influence of N-containing compounds on the 2-electron transfer ORR [28,45]. The profiles of CO and  $\text{CO}_2$  release on TPD-MS (Fig. S4) revealed the presence of O-containing groups for CBox material with relatively large amounts of  $\text{CO}_2$  evolving groups (attributed to carboxylic acids and anhydrides of acidic nature) for CBox compared to CB [46]. A similar trend was observed for CO-releasing groups, associated with the presence of carbonyl, phenolic, and quinone-type groups in CBox. These results are in accordance with those obtained by XPS where the presence of carbonyl groups on the surface of CBox was shown. Furthermore, the presence of these oxygen functional groups led to an increase of the acidity which is corroborated by a decrease of surface pH values from 8.1 to 5.4 after the oxidation of CB by  $\text{HNO}_3$

**Table 2**

Surface pH, and C and O atomic percentage of CB and CBox materials. Values obtained from the XPS are expressed in % of total atomic surface concentration.

Material	Surface pH	C at. % (XPS)	O at. % (XPS)	O/C ratio
CB	8.1	98.3	1.7	0.02
CBox	5.4	91.5	8.5	0.09



**Scheme 1.** Elements of the all-in-one station.

treatment (see Table 2).

The electrochemical behaviour of CB and CBox materials by CV was explored in Ar and O<sub>2</sub>-saturated Na<sub>2</sub>SO<sub>4</sub> solutions (Fig. S5). Under deaerated conditions, the GCE-CB displayed a CV with a narrow current intensity in the region dominated by capacitive processes typically related to the carbonaceous materials with low or none porosity, showing a quasi-rectangular shape thereby denoting the absence of iR drops linked presumably to higher electrical conductivity of CB. GCE-CBox, interestingly, revealed a notably greater double-layer capacitance compared to that one exhibited by the CB-based electrode mainly associated with the increase in the accessibility of electrolyte within surface area and improved hydrophilicity because of the incorporation of oxygen-functionalized groups. Furthermore, the presence of these likely oxygen-containing functionalities was confirmed by the observation of broad reversible pseudo-faradaic peaks at the potential range between ca. 0.20 and 0.50 V vs. Ag/AgCl [41–43]. Under an O<sub>2</sub>-saturated solution (Fig. S5B), both materials exhibit a marked irreversible cathodic peak associated with ORR, which is centered at ca. –0.30 and –0.20 V vs. Ag/AgCl for the GCE-CB and GCE-CBox, respectively. This positive displacement is also observed on LSV performed on a rotating disk electrode (RDE), revealing an onset potential of –0.07 V and –0.16 V vs. Ag/AgCl for CBox and CB, respectively, at 1600 rpm of rotating rate (Fig. S6). This positive shifting obtained for the CBox material suggests that O-functional groups incorporated into the carbonaceous surface, i. e., carbonyl and carboxyl groups, display more significant electrocatalytic activity toward ORR.

The electrocatalytic activity of ORR was explored to elucidate the best cathode for two-electron ORR towards H<sub>2</sub>O<sub>2</sub> generation. Fig. 1 depicts the LSV of both CB- and CBox-based electrodes (CC-CB and CC-CBox) at 5 mV/s in Ar- and O<sub>2</sub>-saturated solutions by performing a potential excursion from 0 V to –1.0 V vs. Ag/AgCl. It is of notice that the ORR response of the CC-PTFE is also recorded for comparative purposes. As seen, in Ar-saturated solution, no faradaic current intensity was observed until a potential of ca. –0.80 V vs. Ag/AgCl set at a current density of 1 mA where hydrogen evolution reaction (HER) takes place [47]. Under O<sub>2</sub>-saturated conditions the LSV shows a larger cathodic current intensity with a marked onset potential for both cathodes at ca. –0.30 V and –0.20 V vs. Ag/AgCl for CC-CB and CC-CBox, respectively. These values are in concordance with the onset potentials and the peak potential observed in the CV behaviour of both materials (Fig. S5). Beyond the onset potential, the current intensity value increases

markedly for both carbonaceous electrodes without the appearance of evident cathodic limit current or cathodic wave associated with two or four-electron ORR before the HER. Current intensities of 16 and 46 mA were recorded at –0.7 V vs. Ag/AgCl for CC-CB and CC-CBox, respectively, (while 2 mA were recorded for CC-PTFE) pointing out the highest catalytic performance of CBox in comparison to that of CB. It should be mentioned that at potentials more negative than –0.7 V, the HER starts to compete with ORR (as was seen in the results obtained from Ar-saturated LSV), slightly increasing the total net current.

With an aim of avoiding biased interpretation of the generated current intensity associated with the different cathodes' area, the electrochemically active surface area (ECSA) measurement was carried out for both the CC-CB and CC-CBox electrodes by deriving a double layer capacitance from CV curves (Fig. S7). As expected, CC-CBox unveils a higher ECSA value than that of CC-CB (i.e., 15.4 and 33.0 cm<sup>2</sup> for CC-CB and CC-CBox, respectively). In order to take into account the effect of the ECSA on the current intensities obtained in Fig. 1, the normalized LSV of both electrodes -current density in mA/cm<sup>2</sup> over applied potential-is depicted in Fig. S8 again revealing a lower onset potential and larger current density for the electrode CC-CBox, confirming that the introduction of O-containing groups into the carbon structures creates structural defects and new active sites that boost ORR in acidic medium.

### 3.2. H<sub>2</sub>O<sub>2</sub> production for 2PP degradation

#### 3.2.1. H<sub>2</sub>O<sub>2</sub> electrogeneration

At this point, we need to reconsider whether the 2e- ORR is a dominant pathway within a specific potential range and whether hydrogen peroxide yield and production rate are remarkable high as a function of electrode potentials. In this regard, Fig. 2 depicts the H<sub>2</sub>O<sub>2</sub> production rate obtained during the electrolysis for studied cathodes when applying different potentials (selected according to LSV responses shown in Fig. 1) in the range of –0.5 and –1.0 V vs. Ag/AgCl during 30 min of electrolysis. Results reveal a notable increase in the H<sub>2</sub>O<sub>2</sub> production rate after incorporating carbonaceous material onto the carbon cloth at all studied potentials, especially in the case of CBox. Additionally, in all the cathodes, the production rate increases monotonically with applied negative potentials, which is in concordance with the largest current measured in the LSV curves.

Hence, it seems evident that the introduction of oxygenated groups improves the 2e- ORR due to: i) easier O<sub>2</sub> adsorption on the surface's electrode, ii) the highest hydrophilic character of the cathode due to the presence of –COOH and C–OH groups, facilitating the O<sub>2</sub> diffusion or approach, and iii) increase of the active sites favouring the reaction efficiency [33,44,48,49]. Production rate values of H<sub>2</sub>O<sub>2</sub> (in the range of 0.5 and 1.2 mg/h cm<sup>2</sup>) are in the same order as those reported for floating air cathodes modified with carbon black/activated carbon [49], carbon black-PTFE [50] and carbon black modified with tert-butyl-anthraquinone [51] gas diffusion cathodes. However, our findings are far from those reported by air-calcined carbon black-based floating air electrodes with productions up to 5 mg/h cm<sup>2</sup> [35] at an applied potential of –1.0 V vs. Ag/AgCl.

Fig. 2B shows the accumulated H<sub>2</sub>O<sub>2</sub> production profiles generated with the tested cathodes by applying a constant electrode potential of –0.7 V vs. Ag/AgCl up to 2 h. In both cathodes, a linear increase is observed at the first stage of the reaction, i.e., up to reach ca. 30–50 min, and subsequently, a decline in increase of H<sub>2</sub>O<sub>2</sub> concentration occurs reaching a somewhat plateau. This behaviour can be ascribed to the participation of side reactions associated with the H<sub>2</sub>O<sub>2</sub> self-decomposition either on the anode or in the bulk solution or its reduction at the cathode [52,53]. This is also linked with the coulombic efficiency (Table S1), which generally drops with longer times of reaction, being more noticeable for the highest potentials applied. It is worth noting that H<sub>2</sub>O<sub>2</sub> production rates at stationary state, i.e., when reaching plateau during electrolysis, results to be almost irrelevant compared to that obtained for CC-CB and CC-CBox electrodes (Fig. S9).

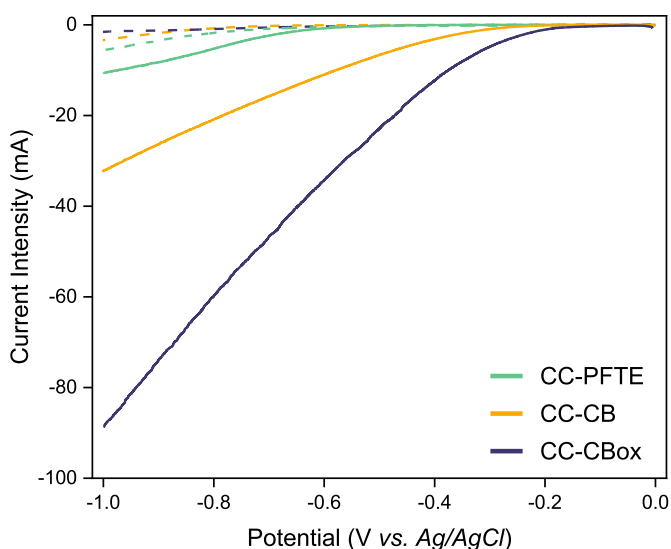
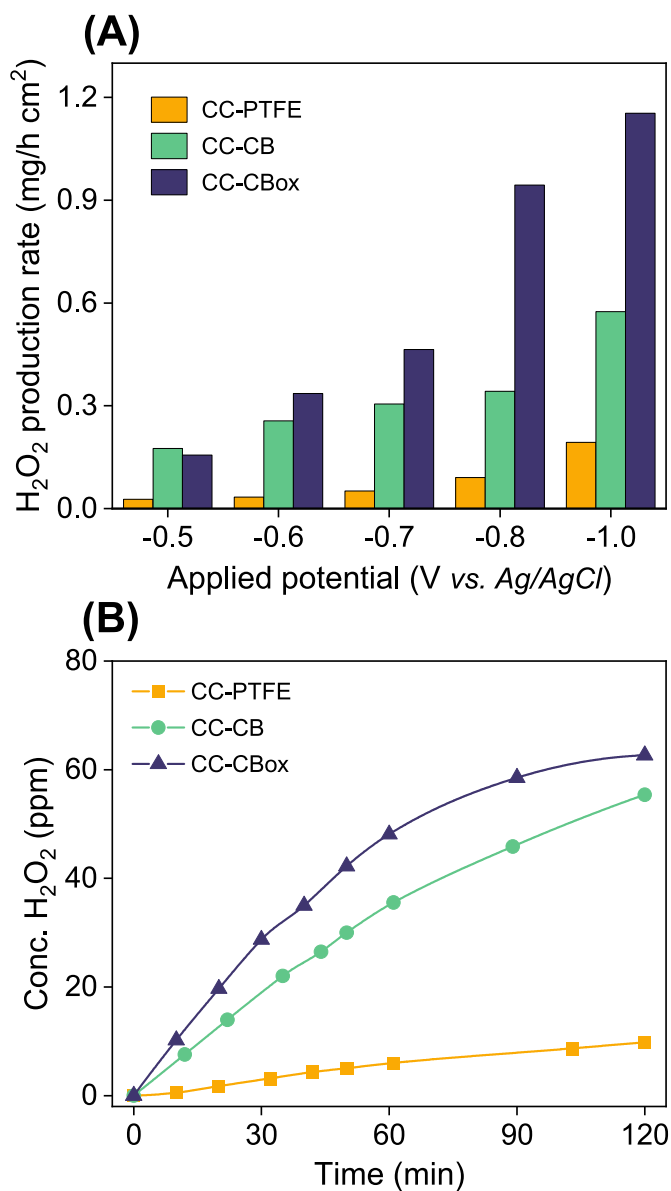


Fig. 1. Linear sweep voltammetry of the electrodes CC-PTFE, CC-CB, and CC-CBox in 50 mM Na<sub>2</sub>SO<sub>4</sub> pH 3.0 under Ar- (dashed line) and O<sub>2</sub>- saturated electrolyte. Scan rate: 5 mV/s.



**Fig. 2.** (A) H<sub>2</sub>O<sub>2</sub> production rate obtained for CC-PTFE, CC-CB, and CC-CBox electrodes after 30 min of electrolysis at different potentials. (B) H<sub>2</sub>O<sub>2</sub> concentration profiles using CC-PTFE, CC-CB, and CC-CBox electrodes at an applied potential of  $-0.7$  V.

### 3.2.2. Pollutant conversion by electro-Fenton process

Next, we turn out for the feasibility of the fabricated electrodes towards the 2PP degradation by EF. Before doing so, it is worthwhile to consider the previous adsorption process of 2PP on the carbon materials-based electrode with the aim of saturating the cathodes' porosity and avoiding accounting for the organic compound removal from the solution associated with its adsorption into the electrode's porosity (the degradation of 2PP nanoconfined on the porosity is out of the aim of this work).

The effect of contact time on the adsorption of 2PP at all three electrodes, as shown in Fig. S10, revealed a total amount adsorbed of 13, 48, and 40  $\mu\text{g}$  2PP/cm<sup>2</sup> for CC-PTFE, CC-CB, and CC-CBox, respectively, thereby showing a stable 2PP concentration in solution after 30 min (presumably a scenario of saturation of electrode's porosity).

After the pre-adsorption step, the degradation of 2PP was evaluated by applying  $-0.7$  V vs. Ag/AgCl as the potential of reference since the production rate of H<sub>2</sub>O<sub>2</sub> is very similar for both carbonaceous electrodes as a function of time, so that the 2PP degradation may be decoupled

from the influence the effect of porosity and nature chemistry onto the surface of CB material; also the participation of HER is discarded at the selected potential.

Fig. 3A shows the degradation rate of the pollutant for the three studied electrodes exhibiting a notable improvement of degradation observed when CB and CBox were incorporated into the carbon cloth. For the modified cloths, the 2PP removal was increasing from 19.2% for CC-PTFE to 34.4 % and 90.0 % for CC-CB and CC-CBox, respectively, after 5 min of electrochemical reaction (Table 3). The reaction rate constants obtained adjusting curves to a pseudo-first-order equation, were 0.36 ( $R^2 = 0.994$ ), 0.11 ( $R^2 = 0.996$ ), and 0.06  $\text{min}^{-1}$  ( $R^2 = 0.993$ ) for CC-CBox, CC-CB and CC-PTFE, respectively.

These results pointed out the catalytic character of the carbon black-based materials being the most catalytic the CC-CBox electrode, which is able to reach 100 % 2PP degradation after 7 min of reaction, while for CC-PTFE more than 60 min are needed for removing the pollutant from the solution. The highest 2PP conversion via HEF reaction obtained for the oxidised material is attributed to the beneficial presence of oxygen-containing functional groups (mainly carboxyl, hydroxyl, and quinones) that also facilitates the electron transfer for Fe<sup>3+</sup> reduction, acting as active sites allowing the Fe<sup>2+</sup> regeneration which improves the catalytic

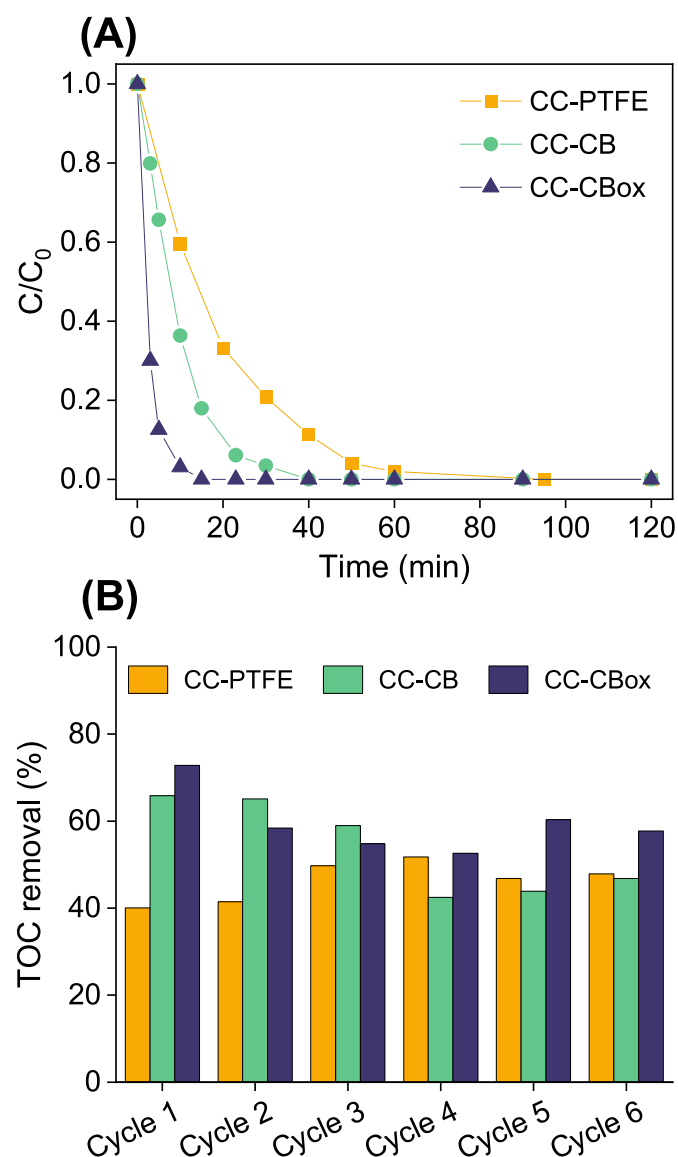


**Fig. 3.** (A) 2PP conversion profiles by HEF on the studied electrodes at  $-0.7$  V vs. Ag/AgCl and (B) TOC removal percentage during 6 consecutive cycles.

**Table 3**

2PP removal percentage after 5 and 30 min of reaction performed at  $-0.7$  V vs. Ag/AgCl, TOC removal after 60 min of reaction, and energy consumption for 2PP degradation for CC-PTFE, CC-CB, and CC-CBox electrodes.

Electrode	2PP removal (%)		TOC removal (%)	Energy Consumption (W h/g 2PP)	
	5 min	30 min		after 5 min of HEF reaction	over 80% 2PP degradation
CC-PTFE	19.2	78.0	40.1	9.0	14.2
CC-CB	34.4	96.5	65.9	4.7	5.8
CC-CBox	90.0	100.0	72.8	5.7	3.9

effect [54].

Even though the conversion of 2PP was fast by the use of CC-CBox electrode, this conversion may result in different organic intermediates (mainly carboxylic acids and quinones or hydroquinones) [55,56]. To evaluate the grade of mineralization of 2PP, TOC was analysed at the end of the HEF reaction. After 60 min of degradation, TOC was removed by 40, 66 and 73 % on CC-PTFE, CC-CB, and CC-CBox, respectively (see compiled data in Table 3). The incomplete mineralization within 60 min suggests that a variety of organic intermediates are still present, being the CBox-based electrode that reaches the higher mineralization degree. This fact points out again that the oxygenated groups not only play a crucial role in the degradation of the pollutant but also display a high efficiency of intermediates degradation. Nonetheless, further investigation is required to clarify the specific role of the oxidised cathode on the degradation pathway.

Table 3 shows the energy consumption per unit mass of 2PP removed for all the three electrodes after a short time of reaction (5 min) and over 80 % of the 2PP conversion. The values were determined by the following equation:

$$EC \left( \frac{kWh}{g} \right) = \frac{U \cdot I \cdot t}{V \cdot \Delta C}$$

where U is the applied cell voltage in V (4.0 V in all experiments), I is the current intensity in A, t is the time in h, V is the solution volume in L, and  $\Delta C$  the variation in the 2PP concentration in ppm. The incorporation of the carbonaceous material into the carbon cloth reduces up to ca. 40 % the energy consumption. However, due to the different electrolysis times required to reach the same conversion percentage, energy consumption is also expressed over 80% of 2PP conversion for comparative purposes, where slightly lower energy consumption for CC-CBox electrode is achieved upon the same conversion grade.

Fig. 3B depicts the reusability of the electrodes through six consecutive HEF reactions by showing the TOC removal after 60 min using CC-PTFE, CC-CB, and CC-CBox electrodes. It might be mentioned that the use of CC-PTFE exhibits small changes over the cycles with a slight increase after the 2<sup>nd</sup> electrolysis (<10 %). In the case of the CC-CB electrode, a decay of ca. 15 % on TOC removal was observed after the 3<sup>rd</sup> electrolysis, and then the TOC removal remained constant for the subsequent reactions. Moreover, for CC-CBox, the maximum TOC removal was observed for the first electrolysis, and thereafter, a decay of the removal percentage was observed from 73 % to 58 % for 1<sup>st</sup> and 2<sup>nd</sup> electrolysis, respectively and, after the second electrolysis, the TOC reduction remains stable. This loss in TOC reduction efficiency could be associated with several factors: i) accumulation of the intermediates and/or the pollutant on the porosity and surface of the carbonaceous cathodes which can inactivate reactive sites for 2e<sup>-</sup> ORR or the regeneration of Fe(II) (although the cathodes are previously saturated with the starting 2PP compound, the applied potential could favour the adsorption-desorption of molecules [57,58] clogging up the active sites); ii) accumulation of the iron cations or Fe complexes on the electrode's surface blocking the catalytic activity, and/or iii) deactivation of the active sites by hydrogen peroxide during consecutive electrolysis. In spite of that, the loss in degradation efficiency after the 1st experiment

for CC-CBox, the TOC removal still attains values above 55 %, higher than those reached by CC-CB, revealing its greater applicability for HEF treatment of 2PP.

### 3.3. Electrochemical behaviour of 2 PP at SPEs

Fig. 4A and B show the CV behaviour of 30 ppm 2PP when performing a scanning of electrode potential from  $-0.30$  until  $0.80$  V vs. Ag/AgCl in 50 mM Na<sub>2</sub>SO<sub>4</sub> pH 3.0 in the presence of 0.2 mM FeSO<sub>4</sub> (the aforementioned working solution for HEF) for both two employed SPEs, SPE-G and SPE-MB. In both electrodes, the redox peaks ascribed to the Fe<sup>2+</sup>/Fe<sup>3+</sup> pair overlapped with the anodic wave of 2PP; nonetheless, current intensity linked to the Fe(II) oxidation is almost negligible according to the current intensities obtained from CV in Fig. S10.

More deeply, for SPE-G (Fig. 4Ai), a sole oxidation peak is observed at 0.60 V during the excursion to positive potentials at the first cycle, showing two cathodic peaks at 0.20 and  $-0.15$  V on the backward to negative potentials. During the second cycle, an extra anodic peak appears at 0.25 V. While the current intensity of the main anodic (at 0.60 V) starts decreasing after successive cycling, the rest of the peaks disappeared after four scans. As a result, over the number of cycles, the electrode is completely blocked, passivated, or fouled caused by polymerization pathways after the eighth cycle, as also reported for the electrooxidation of a similar moiety [59–61]. A complex polymerization mechanism presumably takes place on the electrode surface involving the oxidation of the phenolic ring of 2PP.

Regarding the CV on SPE-MB (Fig. 4Bi), a similar behaviour is obtained with the presence of a main anodic at 0.60 V on the positive scan excursion, and then, two cathodic peaks at 0.22 and  $-0.07$  V appeared after the reverse scan during the first cycle. However, at this electrode, three additional anodic peaks appear at 0.06, 0.26, and 0.36 V, indicating that the oxidation and polymerization process might follow different pathways. Interestingly, the evolution of the CV pattern indicates that at least 40 cycles are needed to reach a complete blocking of the electrode surface, though this can be linked to a bigger current intensity of the main anodic peak at the SPE-MB electrode compared to that one exhibited at SPE-G.

We next turned out to explore the electroanalytical outcomes of 2PP conversion by SWV at both SPE electrodes as shown in Fig. 4ii-iii. Firstly, the SWV response of the electrolyte in the absence and presence of Fe(II) species were recorded since the pair Fe<sup>2+</sup>/Fe<sup>3+</sup> is always present on the HEF-treated solutions (as catalysts). The response of 0.2 mM FeSO<sub>4</sub> (in 50 mM Na<sub>2</sub>SO<sub>4</sub> pH 3.0) at the SPE-G revealed a broad but well-defined anodic peak at ca. 0.55 V vs. Ag/AgCl corresponding to the oxidation reaction of Fe<sup>2+</sup> to Fe<sup>3+</sup>. When 2PP was present in the solution, during the first cycle, an oxidation peak appeared at ca. 0.50 V which overlapped with one of the Fe<sup>2+</sup> oxidation. Shortly thereafter, the reuse of the same SPE-G with a fresh solution, the SWV response unveiled an additional anodic peak centered at ca. 0.2 V. As was already observed on the second cycle of CV, this peak is associated with the generated polymeric-film coming from the oxidation of 2PP. On the consecutive scans (Fig. 4 iii), a prominent shift of the main anodic peak to more positive potentials is observed along with a decrease in current intensity denoting fouling or passivation of the electrode surface.

A similar SWV response is obtained for the electrode SPE-MB which shows first a higher background current intensity when the SWV is recorded for the electrolyte alone, fact that is also observed for the CV experiments (see Fig. S11B). Surprisingly, when using SPE-MB, the anodic oxidation wave associated with Fe<sup>2+</sup> oxidation is not observed when performing the SWV under the same conditions as those ones performed using the SPE-G electrode; this is of analytical importance since 2PP oxidative conversion can be accurately detected without interference. Even though the SPE-MB depicted the same SWV pattern for the 2PP oxidation (1<sup>st</sup> and 2<sup>nd</sup> cycle, see Fig. 4Bii) as that one displayed for the SPE-G electrode, the former revealed a higher stable anodic peak (centered at 0.55 V); beyond the 2<sup>nd</sup> cycle until the 10<sup>th</sup> one



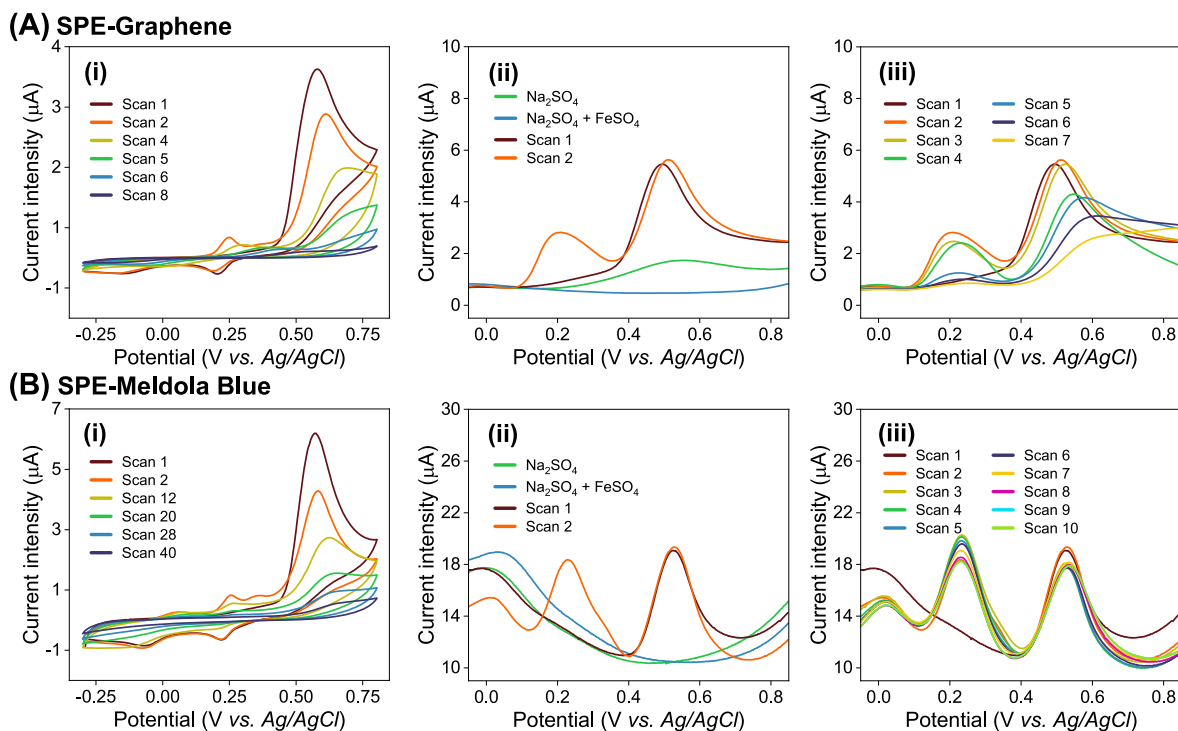


**Fig. 4.** (A) SPE-G and (B) SPE-MB behaviour by (i) cyclic voltammetry with different number of scans of 30 ppm 2PP in 50 mM Na<sub>2</sub>SO<sub>4</sub> pH 3.0 as electrolyte in the presence of 0.2 mM FeSO<sub>4</sub> at electrodes; Scan rate of 20 mV/s (ii) SWV profiles of 30 ppm 2PP in 50 mM Na<sub>2</sub>SO<sub>4</sub> pH 3.0 in the absence and presence of 0.2 mM FeSO<sub>4</sub>. Two consecutive scans are recorded when 2PP is in solution; (iii) depict various SWV measurements when 2PP is in solution. SWV parameters: modulation amplitude, 100 mV; frequency, 8 Hz; modulation step, 2 mV.

showing peak current intensity stability (Fig. 4Biii) with peak area variation lower than 5 % after 10 consecutive SWV experiments. This points out the resistance of the electrode SPE-MB against the fouling or passivated film formation.

In view of the SWV outcomes, SPE-MB was selected as the electrode to follow the 2PP degradation during an HEF reaction due to i) the SWV response of Fe<sup>2+</sup> is not interfering with the potential of study under working conditions; and ii) the higher stability of the SWV response regarding the electrooxidation of 2PP after consecutive measurements.

### 3.4. 2PP sensor and all-in-one device application

Prior to carrying out a HEF coupled with the electrochemical detection of 2PP, the SPE-MB was first validated in terms of sensitivity and range concentration linearity in 50 mM Na<sub>2</sub>SO<sub>4</sub> pH 3.0 in the

presence of 0.2 mM FeSO<sub>4</sub>. Fig. 5 shows SWV responses of 2PP at different concentrations and a calibration plot regarding peak area versus concentration. A good degree of linearity was observed in the range of 0.5–21 ppm with a sensitivity following the next equation:

$$\text{Peak area, SWV} = 3.5 \cdot 10^{-8} \cdot C_{2PP} (\text{ppm}) - 9.1 \cdot 10^{-9}; R^2 = 0.999.$$

The limits of detection (LoD) and quantification (LoQ) were 0.12 ppm and 0.40 ppm, respectively. These values were calculated as three and ten times the noise level, respectively.

Since during the HEF reaction, 2PP concentration is expected to decrease with time, the reversibility within the linear concentration range of the SWV response of the electrode SPE-MB was evaluated by following two consecutive calibration curves performed by increasing and decreasing 2PP standard concentrations (Fig. 5A and B). Reproducible responses were obtained with a relative standard deviation (RSD) of 2.3 % validating the use of the electroanalytical method to be

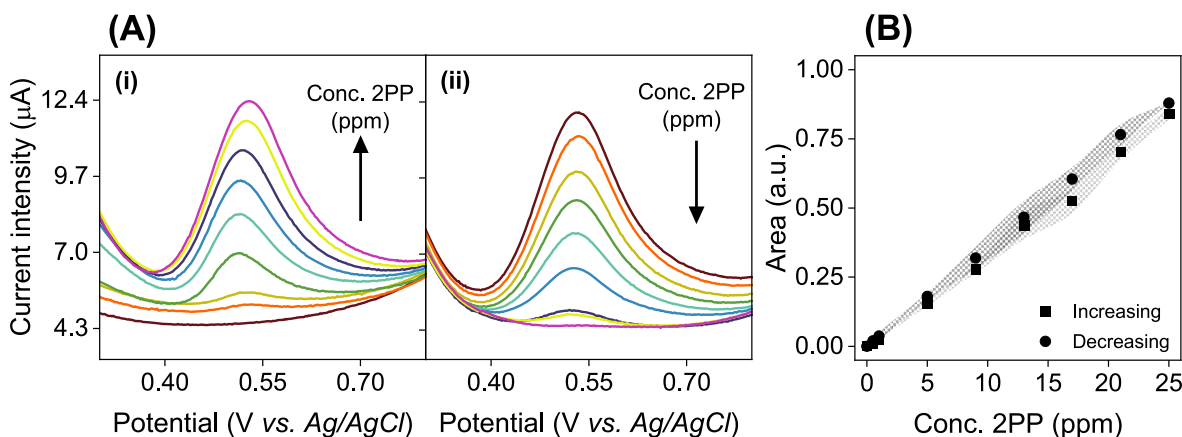


**Fig. 5.** (A) SWV response for increasing and decreasing 2PP concentrations in the range of 0.5–21 ppm in 50 mM Na<sub>2</sub>SO<sub>4</sub> pH 3.0 in the presence of 0.2 mM FeSO<sub>4</sub>. SWV parameters: modulation amplitude, 100 mV; frequency, 8 Hz; modulation step, 2 mV. (B) Calibration curves were obtained.

coupled with HEF reaction evolution.

Scheme 1 (and Fig. S2) illustrates the all-in-one electrochemical station, in which the HEF reactor is coupled to the electrochemical sensor through an inlet and outlet tubes allowing the electroanalytical cell to be filled with the sample by the use of a peristaltic pump. The inner reservoir of the cell has a conic shape to facilitate the circulation of the solution from up to down, favouring the sample transport and therefore minimizing the energy consumption by the pump.

According to the results described in section 3.1, the electrode CC-CBox was chosen to carry out the 2PP degradation by HEF of spiked real samples (i.e., tap water, TW, irrigation water, IW, and spring water, SW). Fig. 6A shows the 2PP conversion profiles performed in three types of waters together with doubled distilled water which is included for comparison purposes. Similar conversion rates were obtained for all tested real aqueous matrices, with a slightly lower conversion rate for IW, probably related to its higher content of chloride and nitrate ions (Table 1), affecting the efficiency of the EF process.

The current trends of the 2PP conversion in spiked real waters were followed by HPLC and the electrochemical sensor based on the use of SPE-MB electrode in the all-in-one electrochemical station. Fig. 6B-E show the SWV response of the treated solution after 1 min of HEF process of the three tested samples as well as DIW. It is worthy of note that for TW and IW a somewhat shift in peak potential is observed for all the SWV towards higher positive potentials, i.e., from 0.55 V (DIW) to 0.63 and 0.67 V for detection peak in TW, and IW, respectively. This shift in peak potentials could be correlated to the higher concentration of chloride ions in both samples. Moreover, no extra peaks or humps were observed in the working potential range for the three tested water samples at any time of HEF reaction indicating that intermediates products obtained from the conversion of 2PP are not interfering with the 2PP electroanalytical outcome.

Table 4 compiles the calculated 2PP concentration obtained from the SPE-MB electrochemical sensor and HPLC for the three samples. Good recovery values were achieved in the range of 100.2–105.6 %, confirming the high reliability of the electrochemical sensor. Table S2 also compiles in more detail the comparative analysis of 2PP conversion using the aforementioned techniques as a function of adsorption and electrolysis time. Overall, the results also pointed out a good performance of the electrochemical sensor with differences between 0.03 and 1.48 ppm (in absolute value) when compared with HPLC, demonstrating the good degree of accuracy of the developed the all-in-one

electrochemical station.

#### 4. Conclusions

The use of carbon black (CB) and its thermally treated in the presence of nitric acid (CBox) have been explored as cathodes for the  $\text{H}_2\text{O}_2$  electrogeneration. The as-obtained CBox, with an increase in the electrochemical active surface area and the incorporation of oxygenated functional groups into the surface, favoured the electrocatalysis towards the two electrons ORR pathway. The use of CBox as a cathode supported on carbon cloths provided high coulombic efficiency and production rate of  $\text{H}_2\text{O}_2$  associated with the highest hydrophilicity of the material facilitating the  $\text{O}_2$  adsorption on the surface's electrode and its diffusion, and to the increase of the number of active sites for the oxygen reaction. In addition, using the CBox based cathode, the HEF process towards the 2PP degradation reached a removal percentage of ca. 90.0 % after 5 min of reaction compared to CB based cathode with a removal of ca. 34.4 %. The all-in-one electrochemical station was designed and validated for the continuous degradation and monitoring of 2PP by using HEF process. The screen-printed electrode modified with Meldola Blue resulted to be an appropriate electrochemical sensor for the detection and accurate quantification of 2PP spiked in real water without any interference of the oxidation of  $\text{Fe}^{2+}$  ions, exhibiting a great 2PP concentration range linearity, sensitivity, LoD and robustness against fouling or blocking of the electrode surface. This work demonstrates that the developed methodology allows the application of an efficient HEF process in real aqueous samples, coupled with continuous electrochemical sensing toward the monitoring of 2PP degradation.

#### CRediT authorship contribution statement

**Alicia Gomis-Berenguer:** Conceptualization, Formal analysis, Investigation, Methodology, Writing – original draft, Writing – review & editing. **Ana Casanova:** Conceptualization, Formal analysis, Investigation, Methodology, Writing – original draft, Writing – review & editing. **Craig E. Banks:** Writing – review & editing. **Jesús Iniesta:** Investigation, Methodology, Writing – review & editing.

#### Declaration of competing interest

The authors declare that they have no known competing financial

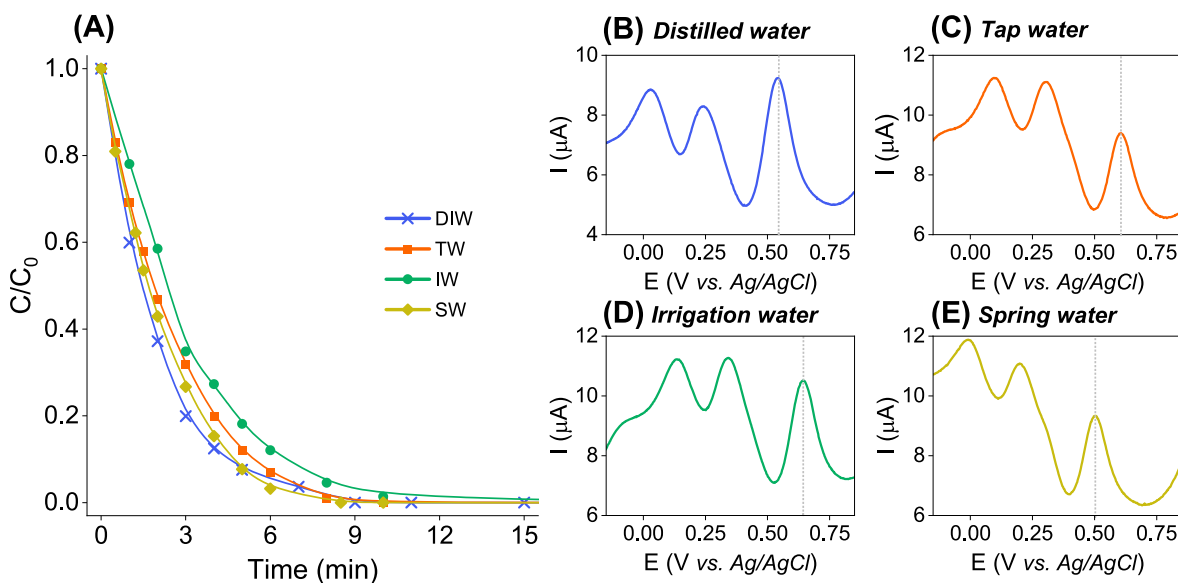


Fig. 6. (A) 2PP conversion monitoring profiles by HEF on the CC-CBox electrode at  $-0.7$  V vs. Ag/AgCl in DIW, TW, IW, and SW solutions. SWV on SPE-MB electrode after 1 min (solid line) and 8 min (dashed line) of HEF treatment in (B) DIW, (C) TW, (D) IW, and (E) SW.

**Table 4**  
2PP determination by HPLC vs. electrochemical sensor.

Process	Tap water, TW			Irrigation water, IW			Spring water, SW		
	[2PP] (ppm)		Diff	[2PP] (ppm)		Diff	[2PP] (ppm)		Diff
	HPLC	Sensor		HPLC	Sensor		HPLC	Sensor	
Initial time	18.84	18.88	-0.04	20.48	21.32	-0.84	20.48	21.62	-1.14
After adsorption	16.98	17.10	-0.12	17.96	17.45	0.51	18.72	19.08	-0.36
5 min HEF	2.04	1.61	0.43	3.04	2.16	0.88	1.44	1.56	-0.12

interests or personal relationships that could have appeared to influence the work reported in this paper.

#### Data availability

Data will be made available on request.

#### Acknowledgments

AG-B thanks European Union NextGenerationEU (ZAMBRANO21-10) for the funding. AC is grateful for the Make Our Planet Great Again fellowship (MOPGA-ref.147446Y) implemented by Campus France and funded by the French Ministry of Foreign Affairs. JI thanks Spanish MINICINN (PID2019-108136RB-C32) for its financial support.

#### Appendix A. Supplementary data

Supplementary data to this article can be found online at <https://doi.org/10.1016/j.talanta.2024.125761>.

#### References

- V.K. Parida, D. Saidulu, A. Majumder, A. Srivastava, B. Gupta, A.K. Gupta, Emerging contaminants in wastewater: a critical review on occurrence, existing legislations, risk assessment, and sustainable treatment alternatives, *J. Environ. Chem. Eng.* 9 (2021) 105966, <https://doi.org/10.1016/j.jece.2021.105966>.
- P. Chaturvedi, P. Shukla, B.S. Giri, P. Chowdhary, R. Chandra, P. Gupta, A. Pandey, Prevalence and hazardous impact of pharmaceutical and personal care products and antibiotics in environment: a review on emerging contaminants, *Environ. Res.* 194 (2021) 110664, <https://doi.org/10.1016/j.envres.2020.110664>.
- H. Uhr, B. Mielke, O. Exner, K.R. Payne, E. Hill, Biocides, *Ullmann's Encyclopedia of Industrial Chemistry*, 2013, pp. 1–26, [https://doi.org/10.1002/14356007.A16\\_563](https://doi.org/10.1002/14356007.A16_563).
- L. Votavová, K. Hanušová, L. Vápenka, J. Dobiáš, F. Kvasnička, Occurrence of 2-Phenylphenol in food paper packages, *Cent. Eur. J. Chem.* 12 (2014) 1162–1168, <https://doi.org/10.2478/S11532-014-0563-X>.
- M. Coelhan, J.T. Yu, A.L. Roberts, Presence of the biocide ortho-phenylphenol in canned soft drinks in the United States and Germany, *Food Chem.* 112 (2009) 515–519, <https://doi.org/10.1016/j.foodchem.2008.05.107>.
- U. Bolz, H. Hagenmaier, W. Körner, Phenolic xenoestrogens in surface water, sediments, and sewage sludge from Baden-Württemberg, south-west Germany, *Environ. Pollut.* 115 (2001) 291–301, [https://doi.org/10.1016/S0269-7491\(01\)00100-2](https://doi.org/10.1016/S0269-7491(01)00100-2).
- X. Peng, Y. Yu, C. Tang, J. Tan, Q. Huang, Z. Wang, Occurrence of steroid estrogens, endocrine-disrupting phenols, and acid pharmaceutical residues in urban riverine water of the Pearl River Delta, South China, *Sci. Total Environ.* 397 (2008) 158–166, <https://doi.org/10.1016/j.scitotenv.2008.02.059>.
- A. Nougadère, V. Siroit, J.P. Cravedi, P. Vasseur, C. Feidt, R.J. Fussell, R. Hu, J. C. Leblanc, J. Jean, G. Rivière, X. Sarda, M. Merlo, M. Hulin, Dietary exposure to pesticide residues and associated health risks in infants and young children - results of the French infant total diet study, *Environ. Int.* 137 (2020) 105529, <https://doi.org/10.1016/j.envint.2020.105529>.
- S. Balakrishnan, L. Hasegawa, D.A. Eastmond, The role of urinary pH in o-phenylphenol-induced cytotoxicity and chromosomal damage in the bladders of F344 rats, *Environ. Mol. Mutagen.* 57 (2016) 210–219, <https://doi.org/10.1002/EM.22002>.
- T. Nunoshiba, E. Watanabe, T. Takahashi, Y. Daigaku, S. Ishikawa, M. Mochizuki, A. Ui, T. Enomoto, K. Yamamoto, Ames test-negative carcinogen, ortho-phenyl phenol, binds tubulin and causes aneuploidy in budding yeast, *Mutat. Res.* 617 (2007) 90–97, <https://doi.org/10.1016/j.mrfmmm.2007.01.002>.
- D. Brusick, Analysis of genotoxicity and the carcinogenic mode of action for ortho-phenylphenol, *Environ. Mol. Mutagen.* 45 (2005) 460–481, <https://doi.org/10.1002/EM.20116>.
- H. Wang, W. Deng, M. Shen, G. Yan, W. Zhao, Y. Yang, A laccase Gl-LAC-4 purified from white-rot fungus *Ganoderma lucidum* had a strong ability to degrade and detoxify the alkylphenol pollutants 4-n-octylphenol and 2-phenylphenol, *J. Hazard Mater.* 408 (2021) 124775, <https://doi.org/10.1016/j.jhazmat.2020.124775>.
- X. Wang, Y. Hu, J. Min, S. Li, X. Deng, S. Yuan, X. Zuo, Adsorption characteristics of phenolic compounds on graphene oxide and reduced graphene oxide: a batch experiment combined theory calculation, *Appl. Sci.* 8 (2018) 1950, <https://doi.org/10.3390/APP8101950>.
- E. Partlan, Y. Ren, O.G. Apul, D.A. Ladner, T. Karanfil, Adsorption kinetics of synthetic organic contaminants onto superfine powdered activated carbon, *Chemosphere* 253 (2020) 126628, <https://doi.org/10.1016/j.chemosphere.2020.126628>.
- A.A. Khodja, T. Sehili, J.F. Pilichowski, P. Boule, Photocatalytic degradation of 2-phenylphenol on TiO<sub>2</sub> and ZnO in aqueous suspensions, *J. Photochem. Photobiol. Chem.* 141 (2001) 231–239, [https://doi.org/10.1016/S1010-6030\(01\)00423-3](https://doi.org/10.1016/S1010-6030(01)00423-3).
- R. Hu, X. Xiao, S. Tu, X. Zuo, J. Nan, Synthesis of flower-like heterostructured β-Bi<sub>2</sub>O<sub>3</sub>/Bi<sub>2</sub>O<sub>3</sub>CO<sub>3</sub> microspheres using Bi<sub>2</sub>O<sub>3</sub>CO<sub>3</sub> self-sacrifice precursor and its visible-light-induced photocatalytic degradation of o-phenylphenol, *Appl. Catal., B* 163 (2015) 510–519, <https://doi.org/10.1016/j.apcatb.2014.08.025>.
- J. Hou, X. Li, J. Li, J. Sun, S. Zheng, Enhanced adsorption of o-phenylphenol on zeolites: a combing pore filling and hydrophobic effects, *Microporous Mesoporous Mater.* 294 (2020) 109860, <https://doi.org/10.1016/j.micromeso.2019.109860>.
- M. Olak-Kucharczyk, S. Ledakowicz, Advanced oxidation of preservative agents in H<sub>2</sub>O<sub>2</sub>/UVC system – kinetics study, transformation products and toxicity assessment, *J. Hazard Mater.* 333 (2017) 348–357, <https://doi.org/10.1016/j.jhazmat.2017.03.047>.
- N. Oturan, J. Bo, C. Trellu, M.A. Oturan, Comparative performance of ten electrodes in electro-Fenton process for removal of organic pollutants from water, *Chemelectrochem* 8 (2021) 3294–3303, <https://doi.org/10.1002/CELC.202100588>.
- V. Poza-Nogueiras, Á. Moratalla, M. Pazos, Á. Sanromán, C. Sáez, M.A. Rodrigo, Towards a More Realistic Heterogeneous Electro-Fenton, 2021, <https://doi.org/10.1016/j.jelechem.2021.115475>.
- K. Wang, J. Huang, H. Chen, Y. Wang, S. Song, Recent advances in electrochemical 2e oxygen reduction reaction for on-site hydrogen peroxide production and beyond, *Chem. Commun.* 56 (2020) 12109–12121, <https://doi.org/10.1039/D0CC05156J>.
- M. Panizza, M.A. Oturan, Degradation of Alizarin Red by electro-Fenton process using a graphite-felt cathode, *Electrochim. Acta* 56 (2011) 7084–7087, <https://doi.org/10.1016/j.electacta.2011.05.105>.
- D. Song, J. Li, Z. Wang, C. Zhao, Performance of graphite felt as anodes in the electro-Fenton oxidation systems: changes in catalysis, conductivity and adsorption properties, *Appl. Surf. Sci.* 532 (2020) 147450, <https://doi.org/10.1016/j.apsusc.2020.147450>.
- Q. Li, C. Batchelor-Mcauley, N.S. Lawrence, R.S. Hartshorne, C.J.V. Jones, R. G. Compton, A flow system for hydrogen peroxide production at reticulated vitreous carbon via electroreduction of oxygen, *J. Solid State Electrochem.* 18 (2014) 1215–1221, <https://doi.org/10.1007/s10008-013-2250-9/TABLES/3>.
- B. Ramirez-Pereda, A. Alvarez-Gallegos, J.G. Rangel-Peraza, Y.A. Bustos-Terrones, Kinetics of Acid Orange 7 oxidation by using carbon fiber and reticulated vitreous carbon in an electro-Fenton process, *J. Environ. Manag.* 213 (2018) 279–287, <https://doi.org/10.1016/j.jenvman.2018.01.022>.
- A. Ozcan, Y. Şahin, A. Savaş Koparal, M.A. Oturan, Carbon sponge as a new cathode material for the electro-Fenton process: comparison with carbon felt cathode and application to degradation of synthetic dye basic blue 3 in aqueous medium, *J. Electroanal. Chem.* 616 (2008) 71–78, <https://doi.org/10.1016/j.jelechem.2008.01.002>.
- A.R. Khataee, M. Safarpour, M. Zarei, S. Aber, Electrochemical generation of H<sub>2</sub>O<sub>2</sub> using immobilized carbon nanotubes on graphite electrode fed with air: investigation of operational parameters, *J. Electroanal. Chem.* 659 (2011) 63–68, <https://doi.org/10.1016/j.jelechem.2011.05.002>.
- J. Park, Y. Nabae, T. Hayakawa, M.A. Kakimoto, Highly selective two-electron oxygen reduction catalyzed by mesoporous nitrogen-doped carbon, *ACS Catal.* 4 (2014) 3749–3754, <https://doi.org/10.1021/CS5008206>.
- Z. Lu, G. Chen, S. Siahrostami, Z. Chen, K. Liu, J. Xie, L. Liao, T. Wu, Di Lin, Y. Liu, T.F. Jaramillo, J.K. Nørskov, Y. Cui, High-efficiency oxygen reduction to hydrogen peroxide catalysed by oxidized carbon materials, *Nat. Catal.* 1 (2) (2018) 156–162, <https://doi.org/10.1038/s41929-017-0017-x>, 1 (2018).
- S. Chen, Z. Chen, S. Siahrostami, D. Higgins, D. Nordlund, D. Sokaras, T.R. Kim, Y. Liu, X. Yan, E. Nilsson, R. Sinclair, J.K. Nørskov, T.F. Jaramillo, Z. Bao, Designing boron nitride islands in carbon materials for efficient electrochemical synthesis of hydrogen peroxide, *J. Am. Chem. Soc.* 140 (2018) 7851–7859, <https://doi.org/10.1021/JACS.8B02798>.

- [31] T. Osaka, X. Liu, M. Nojima, Acetylene black/poly(vinylidene fluoride) gel electrolyte composite electrode for an electric double-layer capacitor, *J. Power Sources* 74 (1998) 122–128, [https://doi.org/10.1016/S0378-7753\(98\)00043-3](https://doi.org/10.1016/S0378-7753(98)00043-3).
- [32] A. Casanova, A. Gomis-Berenguer, A. Canizares, P. Simon, D. Calzada, C.O. Ania, Carbon black as conductive additive and structural director of porous carbon gels, *Materials* 13 (2020) 217, <https://doi.org/10.3390/MA13010217>.
- [33] M.H.M.T. Assumpção, R.F.B. De Souza, D.C. Rascio, J.C.M. Silva, M.L. Calegario, I. Gaubeur, T.R.L.C. Paixão, P. Hammer, M.R.V. Lanza, M.C. Santos, A comparative study of the electrogeneration of hydrogen peroxide using Vulcan and Printex carbon supports, *Carbon* 49 (2011) 2842–2851, <https://doi.org/10.1016/J.CARBON.2011.03.014>.
- [34] J.F. Pérez, C. Sáez, J. Llanos, P. Cañizares, C. López, M.A. Rodrigo, Improving the efficiency of carbon cloth for the electrogeneration of H<sub>2</sub>O<sub>2</sub>: role of polytetrafluoroethylene and carbon black loading, *Ind. Eng. Chem. Res.* 56 (2017) 12588–12595, <https://doi.org/10.1021/ACS.IECR.7B02563>.
- [35] H. Zhang, Y. Li, G. Li, F. Zhang, Scaling up floating air cathodes for energy-efficient H<sub>2</sub>O<sub>2</sub> generation and electrochemical advanced oxidation processes, *Electrochim. Acta* 299 (2019) 273–280, <https://doi.org/10.1016/J.ELECTACTA.2019.01.010>.
- [36] B. Bouzayani, E. Bocos, S.C. Elaoud, M. Pazos, M.A. Sanromán, E. González-Romero, An effective electroanalytical approach for the monitoring of electroactive dyes and intermediate products formed in electro-Fenton treatment, *J. Electroanal. Chem.* 808 (2018) 403–411, <https://doi.org/10.1016/J.JELECHEM.2017.06.035>.
- [37] V. Poza-Nogueiras, M. Arellano, E. Rosales, M. Pazos, M.A. Sanromán, E. González-Romero, Electroanalytical techniques applied to monitoring the electro-Fenton degradation of aromatic imidazolium-based ionic liquids, *J. Appl. Electrochem.* 48 (2018) 1331–1341, <https://doi.org/10.1007/S10800-018-1236-9>.
- [38] A. Fdez-Sanromán, R. Martínez-Treinta, M. Pazos, E. Rosales, M.A. Sanromán, Heterogeneous electro-Fenton-like designs for the disposal of 2-phenylphenol from water, *Appl. Sci.* 11 (2021) 12103, <https://doi.org/10.3390/APP112412103>.
- [39] R.M. Sellers, Spectrophotometric determination of hydrogen peroxide using potassium titanium(IV) oxalate, *Analyst* 105 (1980) 950–954, <https://doi.org/10.1039/AN9800500950>.
- [40] R.O. Kadara, N. Jenkinson, C.E. Banks, Characterization and fabrication of disposable screen printed microelectrodes, *Electrochim. Commun.* 11 (2009) 1377–1380, <https://doi.org/10.1016/J.ELECOM.2009.05.010>.
- [41] K. Kinoshita, J.A.S. Bett, Potentiodynamic analysis of surface oxides on carbon blacks, *Carbon* 11 (1973) 403–411, [https://doi.org/10.1016/0008-6223\(73\)90080-8](https://doi.org/10.1016/0008-6223(73)90080-8).
- [42] B. Avsarala, R. Moore, P. Haldar, Surface oxidation of carbon supports due to potential cycling under PEM fuel cell conditions, *Electrochim. Acta* 55 (2010) 4765–4771, <https://doi.org/10.1016/J.ELECTACTA.2010.03.056>.
- [43] S. Pérez-Rodríguez, E. Pastor, M.J. Lázaro, Electrochemical behavior of the carbon black Vulcan XC-72R: influence of the surface chemistry, *Int. J. Hydrogen Energy* 43 (2018) 7911–7922, <https://doi.org/10.1016/J.IJHYDENE.2018.03.040>.
- [44] A. Moraes, M.H.M.T. Assumpção, F.C. Simões, V.S. Antonin, M.R.V. Lanza, P. Hammer, M.C. Santos, Surface and catalytic effects on treated carbon materials for hydrogen peroxide electrogeneration, *Electrocatalysis* 7 (2016) 60–69, <https://doi.org/10.1007/S12678-015-0279-5>.
- [45] Y. Ding, W. Zhou, J. Gao, F. Sun, G. Zhao, Y. Ding, W. Zhou, J. Gao, F. Sun, G. Zhao, H<sub>2</sub>O<sub>2</sub> electrogeneration from O<sub>2</sub> electroreduction by n-doped carbon materials: a mini-review on preparation methods, selectivity of n sites, and prospects, *Adv. Mater. Interfac.* 8 (2021) 2002091, <https://doi.org/10.1002/ADMI.202002091>.
- [46] J.L. Figueiredo, M.F.R. Pereira, M.M.A. Freitas, J.J.M. Órfão, Modification of the surface chemistry of activated carbons, *Carbon* 37 (1999) 1379–1389, [https://doi.org/10.1016/S0008-6223\(98\)00333-9](https://doi.org/10.1016/S0008-6223(98)00333-9).
- [47] G.A. Oyarzún, K. Bundy, K.B. Westfall, How to minimise hydrogen evolution on carbon based materials? *J. Electrochem. Soc.* 169 (2022) 054516 <https://doi.org/10.1149/1945-7111/ac67f7>.
- [48] J. Miao, H. Zhu, Y. Tang, Y. Chen, P. Wan, Graphite felt electrochemically modified in H<sub>2</sub>SO<sub>4</sub> solution used as a cathode to produce H<sub>2</sub>O<sub>2</sub> for pre-oxidation of drinking water, *Chem. Eng. J.* 250 (2014) 312–318, <https://doi.org/10.1016/J.CEJ.2014.03.043>.
- [49] H. Zhang, Y. Li, Y. Zhao, G. Li, F. Zhang, Carbon black oxidized by air calcination for enhanced H<sub>2</sub>O<sub>2</sub> generation and effective organics degradation, *ACS Appl. Mater. Interfaces* 11 (2019) 27846–27853, <https://doi.org/10.1021/ACSAMI.9B07765>.
- [50] R.D.C. Soltani, A. Rezaee, A.R. Khataee, H. Godini, Electrochemical generation of hydrogen peroxide using carbon black-, carbon nanotube-, and carbon black/carbon nanotube-coated gas-diffusion cathodes: effect of operational parameters and decolorization study, *Res. Chem. Intermed.* 39 (2013) 4277–4286, <https://doi.org/10.1007/S11164-012-0944-8>.
- [51] X. Lu, M. Zhou, Y. Li, P. Su, J. Cai, Y. Pan, Improving the yield of hydrogen peroxide on gas diffusion electrode modified with tert-butyl-anthraquinone on different carbon support, *Electrochim. Acta* 320 (2019) 134552, <https://doi.org/10.1016/J.ELECTACTA.2019.07.063>.
- [52] E. Brillas, R.M. Bastida, E. Llosa, J. Casado, Electrochemical destruction of aniline and 4-chloroaniline for wastewater treatment using a carbon-PTFE O<sub>2</sub> - fed cathode, *J. Electrochem. Soc.* 142 (1995) 1733–1741, <https://doi.org/10.1149/1.2044186>.
- [53] E. Brillas, J.C. Calpe, J. Casado, Mineralization of 2,4-D by advanced electrochemical oxidation processes, *Water Res.* 34 (2000) 2253–2262, [https://doi.org/10.1016/S0043-1354\(99\)00396-6](https://doi.org/10.1016/S0043-1354(99)00396-6).
- [54] F. Deng, H. Olvera-Vargas, M. Zhou, S. Qiu, I. Sirés, E. Brillas, Critical review on the mechanisms of Fe<sup>2+</sup> regeneration in the electro-fenton process: fundamentals and boosting strategies, *Chem. Rev.* 123 (2023) 4635–4662, <https://doi.org/10.1021/ACS.CHEMREV.2C00684>.
- [55] L.S. Andrade, R.C. Rocha-Filho, N. Bocchi, S.R. Biaggio, J. Iniesta, V. García-García, V. Montiel, Degradation of phenol using Co- and Co,F-doped PbO<sub>2</sub> anodes in electrochemical filter-press cells, *J. Hazard Mater.* 153 (2008) 252–260, <https://doi.org/10.1016/J.JHAZMAT.2007.08.046>.
- [56] M. Pimentel, N. Oturan, M. Dezotti, M.A. Oturan, Phenol degradation by advanced electrochemical oxidation process electro-Fenton using a carbon felt cathode, *Appl. Catal., B* 83 (2008) 140–149, <https://doi.org/10.1016/J.APCATB.2008.02.011>.
- [57] A. Puga, M. Pazos, E. Rosales, M.A. Sanromán, Electro-reversible adsorption as a versatile tool for the removal of diclofenac from wastewater, *Chemosphere* 280 (2021) 130778, <https://doi.org/10.1016/J.CHEMOSPHERE.2021.130778>.
- [58] C.O. Ania, F. Béguin, Mechanism of adsorption and electroadsorption of bentazone on activated carbon cloth in aqueous solutions, *Water Res.* 41 (2007) 3372–3380, <https://doi.org/10.1016/J.WATRES.2007.03.031>.
- [59] M. Ferreira, H. Varela, R.M. Torresi, G. Tremiliosi-Filho, Electrode passivation caused by polymerization of different phenolic compounds, *Electrochim. Acta* 52 (2006) 434–442, <https://doi.org/10.1016/J.ELECTACTA.2006.05.025>.
- [60] X. Yang, J. Kirsch, J. Fergus, A. Simonian, Modeling analysis of electrode fouling during electrolysis of phenolic compounds, *Electrochim. Acta* 94 (2013) 259–268, <https://doi.org/10.1016/J.ELECTACTA.2013.01.019>.
- [61] X. Liu, S. You, F. Ma, H. Zhou, Characterization of electrode fouling during electrochemical oxidation of phenolic pollutant, *Front. Environ. Sci. Eng.* 15 (2021) 1–10, <https://doi.org/10.1007/S11783-020-1345-7>.